Astronomy & Astrophysics manuscript no. ltelines
September 10, 2019

Diagnostic capabilities of spectro-polarimetric observations for understanding the solar phenomena I

Zeeman sensitive photospheric lines

C. Quintero Noda[1,2], M. Carlsson[1,2], and P. Barklem[3]

[1] Rosseland Centre for Solar Physics, University of Oslo, P.O. Box 1029 Blindern, N-0315 Oslo, Norway
e-mail: c.q.noda@astro.uio.no
[2] Institute of Theoretical Astrophysics, University of Oslo, P.O. Box 1029 Blindern, N-0315 Oslo, Norway
[3] Theoretical Astrophysics, Department of Physics and Astronomy, Uppsala University, Box 516, 751 20 Uppsala, Sweden

Received ; accepted

ABSTRACT

Lorem ipsum dolor sit amet, consectetuer adipiscing elit. Ut purus elit, vestibulum ut, placerat ac, adipiscing vitae, felis. Curabitur dictum gravida mauris. Nam arcu libero, nonummy eget, consectetuer id, vulputate a, magna. Donec vehicula augue eu neque. Pellentesque habitant morbi tristique senectus et netus et malesuada fames ac turpis egestas. Mauris ut leo. Cras viverra metus rhoncus sem. Nulla et lectus vestibulum urna fringilla ultrices. Phasellus eu tellus sit amet tortor gravida placerat. Integer sapien est, iaculis in, pretium quis, viverra ac, nunc. Praesent eget sem vel leo ultrices bibendum. Aenean faucibus. Morbi dolor nulla, malesuada eu, pulvinar at, mollis ac, nulla. Curabitur auctor semper nulla. Donec varius orci eget risus. Duis nibh mi, congue eu, accumsan eleifend, sagittis quis, diam. Duis eget orci sit amet orci dignissim rutrum.

Key words. Sun: magnetic fields – Techniques: polarimetric – Atmospheric effects – Balloons

1. Introduction

Nulla malesuada porttitor diam. Donec felis erat, congue non, volutpat at, tincidunt tristique, libero. Vivamus viverra fermentum felis. Donec nonummy pellentesque ante. Phasellus adipiscing semper elit. Proin fermentum massa ac quam. Sed diam turpis, molestie vitae, placerat a, molestie nec, leo. Maecenas lacinia. Nam ipsum ligula, eleifend at, accumsan nec, suscipit a, ipsum. Morbi blandit ligula feugiat magna. Nunc eleifend consequat lorem. Sed lacinia nulla vitae enim. Pellentesque tincidunt purus vel magna. Integer non enim. Praesent euismod nunc eu purus. Donec bibendum quam in tellus. Nullam cursus pulvinar lectus. Donec et mi. Nam vulputate metus eu enim. Vestibulum pellentesque felis eu massa.

Quisque ullamcorper placerat ipsum. Cras nibh. Morbi vel justo vitae lacus tincidunt ultrices. Lorem ipsum dolor sit amet, consectetuer adipiscing elit. In hac habitasse platea dictumst. Integer tempus convallis augue. Etiam facilisis. Nunc elementum fermentum wisi. Aenean placerat. Ut imperdiet, enim sed gravida sollicitudin, felis odio placerat quam, ac pulvinar elit purus eget enim. Nunc vitae tortor. Proin tempus nibh sit amet nisl. Vivamus quis tortor vitae risus porta vehicula.

Fusce mauris. Vestibulum luctus nibh at lectus. Sed bibendum, nulla a faucibus semper, leo velit ultricies tellus, ac venenatis arcu wisi vel nisl. Vestibulum diam. Aliquam pellentesque, augue quis sagittis posuere, turpis lacus congue quam, in hendrerit risus eros eget felis. Maecenas eget erat in sapien mattis porttitor. Vestibulum porttitor. Nulla facilisi. Sed a turpis eu lacus commodo facilisis. Morbi fringilla, wisi in dignissim interdum, justo lectus sagittis dui, et vehicula libero dui cursus dui. Mauris tempor ligula sed lacus. Duis cursus enim ut augue. Cras ac magna. Cras nulla. Nulla egestas. Curabitur a leo. Quisque egestas wisi eget nunc. Nam feugiat lacus vel est. Curabitur consectetuer.

2. Methodology

2.1. Spectral lines

2.2. Synthesis of the Stokes profiles

We make use of the SIR code (Stokes inversion based on Response Functions; Ruiz Cobo & del Toro Iniesta 1992) in this work for synthesizing and inverting the full Stokes vector. The code assumes local thermodynamic equilibrium and computes the atomic level populations solving the Saha-Boltzmann equation. The former is a valid approximation for the lines we study in this work (cite) , at the same time, the later property improves the accuracy of the emergent spectra in comparison with faster and simpler approaches like the Milne-Eddington approximation (cite). Mention more details about the spectral resolution...

We use two types of input atmospheric models. First, we start with the semi-empirical HSRA atmosphere (Gingerich et al. 1971). Later, we use snapshot 385 of the enhanced network simulation (Carlsson et al. 2016) computed with the BIFROST code (Gudiksen et al. 2011). We show the spatial distribution of several atmospheric parameters at a geometrical height $Z = 0$ km for the computed full field of view in Figure 1. Regarding the properties of this simulation, we refer the reader to the work of Carlsson et al. (2016). We do not include any spatial degradation in our studies, i.e. we use the original horizontal pixel size of 48 km.

Atom	λ [Å]	log(gf)	L_1	L_2	g_1	g_2	$\bar{g}$	s	d	$\bar{G}$	$I(\lambda_0)$ [au]	d_c	s_Q	s_V
Fe I	5247.0501	-4.946	$^5D_2$	$^7D^o_3$	1.50	1.75	2.00	18.00	-6.00	3.98	2808	0.719	1.509	3.152
Fe I	5250.2086	-4.938	$^5D_0$	$^7D^o_1$	0.00	3.00	3.00	2.00	-2.00	9.00	2841	0.715	2.252	7.094
Fe I	5250.6456	-2.181	$^5P_2$	$^5P^o_3$	1.83	1.67	1.50	18.00	-6.00	2.24	2028	0.796	1.254	1.967
Fe I	6173.3352	-2.880	$^5P_1$	$^5D^o_0$	2.50	0.00	2.50	2.00	2.00	6.25	3738	0.626	1.933	5.966
Fe I	6301.5008	-0.718	$^5P^o_2$	$^5D_2$	1.83	1.50	1.67	12.00	0.00	2.52	2780	0.722	1.520	2.890
Fe I	6302.4932	-1.131*	$^5P^o_1$	$^5D_0$	2.50	0.00	2.50	2.00	2.00	6.25	3443	0.656	2.066	6.511
Fe I	6733.1508	-1.580*	$^5P^o_1$	$^5D_0$	2.50	0.00	2.50	2.00	2.00	6.25	7530	0.247	0.832	2.800
Fe I	6820.3715	-1.290	$^5P^o_1$	$^5P_2$	2.50	1.83	1.50	8.00	-4.00	2.18	6453	0.355	0.726	1.439
Fe I	6842.6854	-1.290	$^5P^o_1$	$^5P_1$	2.50	2.50	2.50	4.00	0.00	6.25	6589	0.341	1.167	3.992
Fe I	8468.4069	-2.072	$^5P_1$	$^5P^o_1$	2.50	2.50	2.50	4.00	0.00	6.25	3643	0.636	2.691	11.40
Fe I	8514.0716	-2.229	$^5P_2$	$^5P^o_2$	1.83	1.83	1.83	12.00	0.00	3.36	3813	0.619	1.928	6.027
Fe I	10783.051	-2.571*	$^3P_0$	$^3P^o_1$	0.00	1.50	1.50	2.00	-2.00	2.25	6877	0.312	1.010	3.268
Si I	10786.856	-0.365	$^3P^o_1$	$^3P_0$	1.50	0.00	1.50	2.00	2.00	2.25	3906	0.609	1.972	6.382
Fe I	15534.246	-0.585*	$^5D_1$	$^5P^o_2$	1.50	1.83	2.00	8.00	-4.00	3.98	6606	0.339	2.109	13.04
Fe I	15542.083	-0.457*	$^5D_1$	$^5D^o_0$	1.50	0.00	1.50	2.00	2.00	2.25	7157	0.284	1.326	6.181
Fe I	15648.514	-0.714*	$^7D_1$	$^7D^o_1$	3.00	3.00	3.00	4.00	0.00	9.00	7003	0.300	2.814	26.42

Table 1. The log gf values were obtained from the NIST data base too except for the spectral lines Fe I 6302.5 Å that were taken from the Kurucz linelist database.

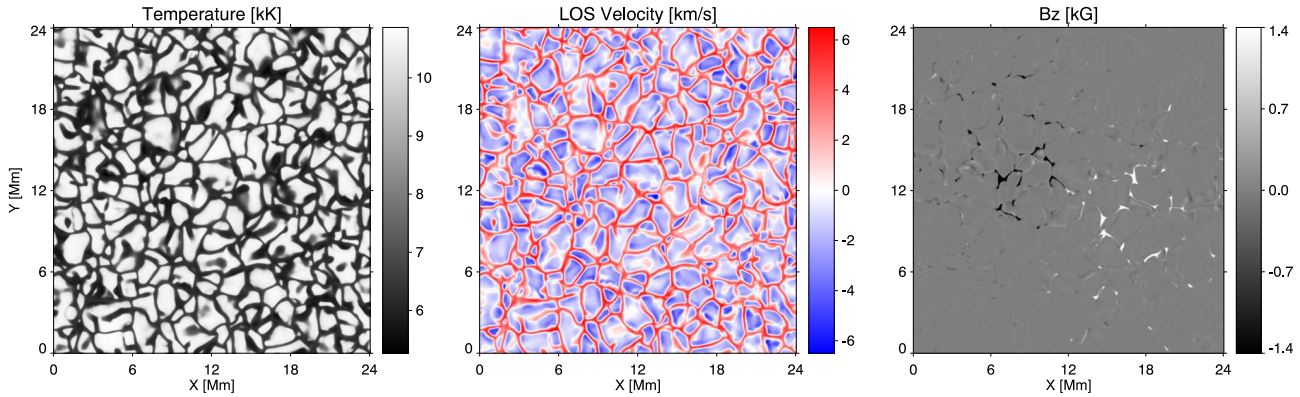

Fig. 1. Snapshot 385 from the BIFROST enhanced network simulation. From left to right, temperature, LOS velocity, and longitudinal field strength at the geometrical height $Z = 0$ km.

2.2.1. Auxiliary lines

There are a few spectral lines that we have included in Table 1 that are strictly not the best candidates for Zeeman polarimetry, e.g. their effective Landé factor is not as large as the others or they do not present particular properties in certain magnetic configurations. However, they are similar to those that are very sensitive to the magnetic field and they were used in the past for estimating, for instance, the field strength of quiet Sun observations (**?**). In the mentioned work, the authors computed the ratio between Fe I 5247 and 5250.2 Å lines as the levels that produced their transitions are identical except for the total angular momentum values. This allowed them to infer the field strength form the Stokes V amplitude ratio since the difference between both lines should be the Landé factor. Hence, it was customary to observe them together and we expect that some observers will do the same with future facilities. In that sense, we also included the Fe I 8468 and 8515 Å as they represent a similar case. Being, in addition, the later located between the two Ca II 8498 and 8542 Å lines. In other words, the later line, by itself would represent and excellent photospheric complement to the two chromospheric lines from the infrared triplet. We also added the two Fe I 10783 and Si I 10876 Å lines as they are closely located to be observed together and can complement each other. Finally, we described in Table 2 additional lines that fall close to the target spectral line of this work and usually observed together, i.e. Fe I 5250.6 and 6301.5 Å.

2.3. Collisions with neutral hydrogen

We compute the line broadening cross sections for the broadening of spectral lines by collisions with neutral hydrogen atoms using the abo-cross calculator (Barklem et al. 2015). The description of the theory and how to use the code can be found in (Barklem et al. 1998). However, for the sake of clarity, we will describe here a few examples where the definition of the input values is not straightforward. We show in Table 2 the parameters we used for the transitions of interest in this work as well as the output from the calculator, i.e. the cross section σ and the velocity parameter α. We have included the target lines of this work and also additional transitions that fall close to the spectral lines of interest. The reason is because in most of the observa-

Atom	λ [Å]	Lower term	Upper term	E_{lower}	E^{limit}_{lower}	E_{upper}	E^{limit}_{upper}	L_{low}	L_{upp}	J_{low}	J_{upp}	σ	α
Fe I	5247.0501	$3d^6(^5D)4s^2$ a ^{5}D 2	$3d^6(^5D)4s4p(^3P^o)$ z $^7D^o$ 3	704.007	63737.704	20019.635	63737.704	0	1	2	3	206.44	0.253
Fe I	5250.2086	$3d^6(^5D)4s^2$ a ^{5}D 0	$3d^6(^5D)4s4p(^3P^o)$ z $^7D^o$ 1	978.074	63737.704	19757.032	63737.704	0	1	0	1	206.91	0.253
Fe I	5250.6456	$3d^7(^4P)4s$ a ^{5}P 2	$3d^6(^5D)4s4p(^1P^o)$ y $^5P^o$ 3	17726.988	76933.840	36766.966	63578.161	0	1	2	3	342.90	0.267
Fe I	6173.3352	$3d^7(^4P)4s$ a ^{5}P 1	$3d^7(^4F)4p$ y $^5D^o$ 0	17927.382	76933.840	34121.603	65738.010	0	1	1	0	279.56	0.265
Fe I	6301.5008	$3d^6(^5D)4s4p(^3P^o)$ z $^5P^o$ 2	$3d^6(^5D)4s(^6D)5s$ e ^{5}D 2	29469.024	63737.704	45333.875	63737.704	1	0	2	2	832.34	0.243
Fe I	6302.4932	$3d^6(^5D)4s4p(^3P^o)$ z $^5P^o$ 1	$3d^6(^5D)4s(^6D)5s$ e ^{5}D 0	29732.736	63737.704	45595.086	63737.704	1	0	1	0	847.73	0.240
Fe I	6733.1508	$3d^6(^5D)4s4p(^1P^o)$ y $^5P^o$ 1	$3d^6(^5D)4s(^4D)5s$ g ^{5}D 0	37409.555	63737.704	52257.346	63737.704	1	0	1	0	——	——
Fe I	6820.3715	$3d^6(^5D)4s4p(^1P^o)$ y $^5P^o$ 1	$3d^6(^5D)4s(^6D)4d$ e ^{5}P 2	37409.555	63737.704	52067.469	63737.704	1	2	1	2	897.36	0.279
Fe I	6842.6854	$3d^6(^5D)4s4p(^1P^o)$ y $^5P^o$ 1	$3d^6(^5D)4s(^6D)4d$ e ^{5}P 1	37409.555	63737.704	52019.669	63737.704	1	2	1	1	890.81	0.278
Fe I	8468.4069	$3d^7(^4P)4s$ a ^{5}P 1	$3d^6(^5D)4s4p(^3P^o)$ z $^5P^o$ 1	17927.382	76933.840	29732.736	63737.704	0	1	1	1	258.79	0.247
Ti I	8468.4700	$3d^3(^2G)4s$ a ^{3}G 5	$3d^2(^1D)4s4p(^3P^o)$ x $^3F^o$ 4	15220.393	63912.060	27025.659	63578.161	0	1	5	4	267.81	0.248
Fe I	8514.0716	$3d^7(^4P)4s$ a ^{5}P 2	$3d^6(^5D)4s4p(^3P^o)$ z $^5P^o$ 2	17726.988	76933.840	29469.024	63737.704	0	1	2	2	256.61	0.246
Fe I	10783.051	$3d^7(^2P)4s$ c ^{3}P 0	$3d^6(^5D)4s4p(^3P^o)$ z $^3P^o$ 1	25091.599	81857.423	34362.873	63737.704	0	1	0	1	307.01	0.271
Si I	10786.856	$3s^23p4p$ ^{3}D 2	$3s^23p4d$ $^3F^o$ 2	48102.323	66035.000	57372.297	66035.000	1	2	2	2	1341.48	0.302
Fe I	15534.246	$3d^6(^5D)4s$ (^{6}D)5s e ^{5}D 1	$3d^6(^5D)4s$ (^{6}D)5p u $^5P^o$ 2	45509.152	63737.704	51944.784	63737.704	0	1	1	2	——	——
Fe I	15542.083	$3d^6(^5D)4s$ (^{6}D)5s e ^{5}D 1	$3d^6(^5D)4s$ (^{6}D)5p t $^5D^o$ 0	45509.152	63737.704	51941.540	63737.704	0	1	1	0	——	——
Fe I	15648.514	$3d^6(^5D)4s$ (^{6}D)5s e ^{7}D 1	$3d^6(^5D)4s$ (^{6}D)5p n $^7D^o$ 1	43763.980	63737.704	50152.619	63737.704	0	1	1	1	974.42	0.229

Table 2. Atomic information used for computing the collisional broadening parameters. From left to right, the atom species, transition wavelength (in), the spectroscopic configuration for the lower and upper term, the energy of lower term, the energy limit of that level, the energy of the upper level, the limit energy of that level, the angular momentum of the lower and upper level, the total angular momentum of the lower and upper level, and the cross section σ and the velocity parameter α. Units for the wavelength are Å, for the energy are in cm^{-1}, and atomic units for the cross section σ, respectively. The velocity parameter α is dimensionless.

tions, those lines are scanned together to complement the most Zeeman sensitive transitions.

We can start with the Fe I 5250.2 Å transition. We extract from the NIST data base (Kramida et al. 2018), the basic information as the the energy of each level (E_{lower} and E_{upper}), the orbital angular momentum (L), and the total angular momentum (J). The only remaining input parameters are the series limit E_{limit}. This energy is defined as the excitation energy and corresponds to energy of the level of interest after removing one electron. In this case, the parent state is $3d^64s$ that corresponds to the ground level of Fe II. Thus, E_{limit} is the excitation energy of Fe I, i.e. 63737.704 cm^{-1}. In the case of the Fe I 5250.6 Å transition, we have that, after removing one electron from the upper level, the term remains like $3d^64s$, so the series energy is again the excitation energy and E_{limit} = 63737.704 cm^{-1}. However, when removing the last electron from the lower level, we have $3d^7(^4$P) that corresponds to the fourth level of Fe II. This means that, the series energy should be the sum of the excitation energy plus the energy of the later level.

This means that, the series energy should be the sum of the excitation energy plus the energy of the later level. There are different ways to include this correction but we believe the simplest one is to add the term energy of that level (also provided by the NIST data base) instead of working out which J values are actually relevant and, then, statistically average only those. The reason why believe it is enough is because the second option supposes a small change that is well below the accuracy of the theory so we prefer to simply take the averaged term energy. In this case, we have that NIST gives a term energy for $3d^7(^4$P) of 13196.137 cm^{-1}. This means that the series energy of the lower level is E_{limit} = 63737.704 + 13196.137 = 76933.840 cm^{-1}. Just for completeness, we describe an additional example where we have the same problem. If we look at the Ti I line at 8468.470 Å, the lower configuration and state are $3d^3(^2$G)$4s$ a ^{3}G. Thus, when the $4s$ electron is removed we have an excited core of Ti II, i.e. different from the ground state of Ti II $3d^2(^3$F)4s a^{4}F, but instead an excited state $3d^3$ a ^{2}G. In this case, the series limit of states arising from the configuration $3d^3(^2$G) is not 55072 cm^{-1}, but 55072.5+8839.5599 = 63912.060 cm^{-1}, where 8839.5599 is, again, the term energy for $3d^3(^2$G) in Ti II. Physically, this means it takes more energy to unbind the outer electron if the core is excited than if the core is not excited, and this is important since it changes the wave function of the outer electron.

As final note,, in the case of the SIR code, the cross section σ needs to be given normalised by the square of the Bohr radius. Thus, we need to multiply the σ values given in the table by $a_0^2 = 2.80028 \times 10^{-17}$ cm^2.

2.4. Auxiliary spectral lines

2.5. Spatial distribution of signals

Acknowledgements

References

Barklem, P. S., Anstee, S. D., & O'Mara, B. J. 1998, PASA, 15, 336

Barklem, P. S., Anstee, S. D., & O'Mara, B. J. 2015, abo-cross: Hydrogen broadening cross-section calculator

Carlsson, M., Hansteen, V. H., Gudiksen, B. V., Leenaarts, J., & De Pontieu, B. 2016, A&A, 585, A4

Gingerich, O., Noyes, R. W., Kalkofen, W., & Cuny, Y. 1971, Sol. Phys., 18, 347

Gudiksen, B. V., Carlsson, M., Hansteen, V. H., et al. 2011, A&A, 531, A154

Kramida, A., Ralchenko, Y., Reader, J., & NIST ASD Team. 2018, NIST Atomic Spectra Database (version 5.6.1), [Online]. Available: `http://physics.nist.gov/asd`

Ruiz Cobo, B. & del Toro Iniesta, J. C. 1992, ApJ, 398, 375